

Global View of Energetic Particles During a Major Magnetic Storm

Timo Asikainen, Kalevi Mursula, Raine Kerttula

Department of Physical Sciences, University of Oulu, Finland

R. Friedel

Los Alamos National Laboratory, Los Alamos, New Mexico

D. Baker

LASP, University of Colorado at Boulder

F. Søråas

University of Bergen, Norway

J. F. Fennell, J. B. Blake

Aerospace Co., Los Angeles, California

We study the global properties of energetic particles during the main and early recovery phase of a major magnetic storm of March 31, 2001, using data of the NOAA-15 and 16 and the CLUSTER satellites. During the storm main phase the ring current energetic electron and ion fluxes were increased by nearly two orders of magnitude, and the flux maxima were shifted to below $L = 3$. The maximum ion fluxes were observed at about 04-07 UT, coinciding with the strongly decreasing Dst and maximum Kp. At this time the ring current was dominated by oxygen ions. However, the highest fluxes of energetic electrons were observed at considerably higher L shells and only at about 16-18 UT, in a good correlation with the maximum of the AE index. These observations indicate significant differences in the acceleration of energetic electrons and ions during the storm. We suggest that at least the low energy ring current ion flux maximum at about 04-06 UT is mainly due to the field-aligned acceleration of escaping ionospheric oxygens by electromagnetic ion cyclotron waves, whereas the electron maximum at 16-18 UT is due to a large injection from the nightside.

1. INTRODUCTION

During a geomagnetic storm the inflow of solar wind energy into the magnetosphere is significantly enhanced. This is reflected by an intensified ring current (RC) particularly at $L < 4$ [Smith and Hoffman, 1973; Hamilton et al., 1988]. The location of the RC energy density maximum is correlated with storm intensity. For a moderate storm with a minimum Dst = -120 nT the energy density maximum was found at $L = 3.5$ [Korth and Friedel, 1997] but for a great storm with a minimum Dst = -300 nT it was at $L = 2.5$

[Hamilton et al., 1988]. Also the RC ion content has been found to correlate with storm intensity so that the stronger the storm is, the higher is the ionospheric oxygen contribution to RC. During the main phase of major magnetic storms the oxygen ions can even be the main ion constituent in the ring current [Hamilton et al., 1988; Daglis, 1997].

In this paper we will analyse both electron and proton dynamics during the great storm of March 31, 2001, and show that they depict a surprisingly different behaviour during this storm.

2. INSTRUMENTATION

In this study we use particle data from Cluster and NOAA-15 and 16 satellites. The MEPED (Medium Energy Proton and Electron Detector) instrument onboard the NOAA satellites measures ions (no ion mass separation is provided) and electrons in two directions, roughly vertical (the 0° detector) and roughly horizontal (the 90° detector), with 30° field of view. Note that at high (resp. low) latitudes the 0° detector measures mostly precipitating (trapped) particles and vice versa for the 90° detector. The MEPED instrument has six energy channels for ions (from 30-80 keV to >7000 keV) and three energy channels for electrons (from 30 keV to > 300 keV). Because the heavier ions require more energy to penetrate into the detector the lower energy limit for heavy ions is slightly higher than the nominal value. For oxygen ions the lower energy limit is estimated to be about 45 keV instead of the nominal 30 keV [Søråas et al., 2002]. NOAA-15 and 16 have polar orbits at an altitude of about 850 km. The orbital plane is 20-08 MLT for NOAA-15 and 14-02 MLT for NOAA-16 (see Evans and Greer, 2000, for more details of the MEPED instrument). NOAA auxiliary data include L shell estimates calculated using the IGRF-2000 model, independent of magnetic disturbance level.

Cluster satellites have two instruments for detecting and analyzing ions. The CIS (Cluster Ion Spectrometry) CODIF (COmposition and Distribution Function analyzer) instrument measures the distributions of major plasma ions (H^+ , He^+ , He^{++} and O^+) in the thermal to suprathermal energy range from 0 to 40 keV/e. (A comprehensive description of the CIS instrument properties is given by Réme et al., 1997.) The RAPID (Research with Adaptive Particle Imaging Detectors) spectrometer for the CLUSTER mission analyzes suprathermal plasma distributions in the energy range from 20-400 keV for electrons, 40-1500 keV for protons and 10-1500 keV/nuc for heavier ion species. The RAPID instrument uses two different and independent detector systems for the detection of nuclei and electrons: IIMS (Imaging Ion Mass Spectrometer) and IES (Imaging Electron Spectrometer). (See [Wilken et al., 1997], for a

more detailed description of the RAPID instrument.)

3. OBSERVATIONS

3.1. Storm Overview

On March 31, 2001, the Advanced Composition Explorer (ACE) satellite was measuring interplanetary conditions at about (223, -23, -12) R_E . As shown in Figure 1, IMF B_z (GSM) component was positive from 0030 UT until 0240 UT, then fluctuating between negative and positive values until about 0330 UT when the IMF direction changed southwards for about four hours. Strongest negative values of B_z (<-40 nT) were observed around 06 UT. The solar wind (SW) velocity increased between 00 UT and 02 UT in two steps from about 400 km/s to above 750 km/s. Solar wind dynamic pressure, which mainly followed the changes in SW density, showed dramatic variations during the first six hours of the day. At about 0020 UT, SW pressure had a very sharp peak which lasted only about half an hour. Another, longer period of increased pressure lasted roughly from 02 UT to 06 UT. These interplanetary conditions led to the generation of a major (Dst about -360 nT; see Figure 1) magnetic storm with a rapid main phase starting at 04 UT and ending at 08 UT. Note that, taking the average SW/IMF time delay of about 30-40 min into account, the positive turning of IMF B_z at about 07 UT corresponds very well with the end of the storm main phase at 08 UT. The extreme geomagnetic conditions were also verified by the LANL geostationary satellite data (not shown here), which indicate that the magnetopause was pushed inside the geosynchronous orbit in the dayside roughly at about 03-08 UT and even in the morning and evening sectors at around 06 UT. After a long period of mainly positive values, the IMF B_z experienced another long interval of negative values at about 14-22 UT which caused a secondary minimum in Dst (-285 nT).

The AE index (bottom panel of Figure 1) shows dramatic changes in the intensity of auroral electrojets during the day. The AE index attains fairly high values already in the beginning of the day, exceeding 1000 nT a few times during the first few hours of the day. Note also that the AE index does not depict exceptionally high values during the main phase of the storm, and remains at a rather low level at around 06 UT. The highest values of the AE index of above 2000 nT are observed only after the storm main phase at about 16-21 UT as three enhancements, the first one at about 16-17 UT being the strongest. However, it should be pointed out that during the main phase of a major magnetic storm the auroral currents may descend significantly equatorward of the latitude of AE stations. In this case the AE index underestimates the intensity of auroral electrojet currents. This is also the case at the main phase

of the present storm since the Kp index (measured by mid-latitude stations) shows the maximum of 9- around 06 UT.

3.2. NOAA Observations

Figure 2 shows the total energetic ion and electron fluxes measured by the 90° detectors of NOAA-16 on March 30-31, 2001. (The 0° detector shows the same behavior). The ion and electron fluxes at both detectors are increased by nearly two orders of magnitude from the average level of March 30 to their storm time maxima during the next day. As seen in Figure 2, the maximum ion flux is observed at about 04-07 UT, coinciding with the time of the steepest descent of the Dst index (and maximum Kp). Instead, the maximum flux of electrons is observed only at 16-18 UT, coinciding well with the largest values of the AE index. A secondary maximum in the ion flux and a secondary minimum in the Dst index occur soon thereafter at about 18-19 UT. All these general features are supported by corresponding NOAA-15 data.

Figure 3 shows the 0° and 90° ion flux maxima for the three lowest energy channels of the MEPED instrument during each pass of the NOAA-16 satellite in the post-midnight sector. All channels show two distinct flux enhancements: one around 06 UT and the other at about 1800 UT. The first enhancement is considerably stronger than the second one. Note also that the lowest energy channel shows a different behavior during the first enhancement than the higher energies. In the 30-80 keV energy range the ion fluxes grow faster and reach their maximum already at about 0430 UT. At higher energies the fluxes are relatively small and steady until a large spike-like enhancement occurs at about 0630 UT.

The L-shells of the observed ion flux maxima during each NOAA-16 nightside pass are shown in Figure 4. The general behavior of the different energy channels is fairly similar. The L-shell of the maximum flux shifts inwards as the storm main phase progresses until the maximum flux is observed at the lowest L-shell. This rule seems to be valid in detail so that the lowest energy channel reaches its minimum L-shells first, in accordance with its earlier flux maximum. (Note that there are small differences between the 0° and 90° detectors because of temporal evolution. The 0° detector reaches its maximum earlier in the northern hemisphere at a higher L shell, while the 90° detector maximum is later in the southern hemisphere at a lower L shell. Note also that at low L-shells the 90° detector is closer to the precipitating flux.) This leads to the interesting fact that while the L-shells of flux maxima for different energies are ordered normally, e.g., higher L-shells for smaller energies, at 0430 UT the lowest channel maximum is at lower L-shells than the maxima in the other channels. The normal situation is reached again by the strong enhancement after 06 UT.

Figures 5 and 6 show similar plots for NOAA-15 in the dusk sector as Figures 3 and 4 for NOAA-16. As for NOAA-16 the observed fluxes in NOAA-15 show two broad enhancements: one during the storm main phase and the other at about 18 UT during the recovery phase. Also, as for NOAA-16, interesting differences are found between the three ion energy channels during the main phase. The two highest channels depict a simultaneous enhancement at about 0430 UT that also forms the maximum flux in the highest energy channel during the main phase. This enhancement occurs at about $L=3.7$. However, the L shell of maximum flux is still decreasing at that time and the final, lowest L shell region is obtained only when the lowest energy channel finds its maximum flux. The other energy channels have their maximum flux L -shells in the same region at the same time, not during their respective flux maxima. The second channel has its flux maximum at about 0730 UT which could well be due to the drift of those ions whose flux maximum was found in NOAA-16 at 0630 UT. (The highest energy ions were mainly missed by NOAA-15 because of their faster drift speed and the coarse sampling time. This is supported by the very fast decline of the flux after 0630 UT at NOAA-16, implying a rather limited injection time.) Note that the final minimum L shell (2.8) is the same in NOAA-15 and NOAA-16, giving strong support for the global nature of the observed changes in the magnetosphere, as well as for the credibility of NOAA observations. Finally, we note that the absolute maximum flux of the highest energy ions at NOAA-15 occurs at about 18 UT and is only slightly lower than the corresponding maximum at NOAA-16 at 0630 UT.

The maximum electron fluxes in the two lowest energy channels observed by NOAA-16 for each nightside pass are shown in Figure 7. The two channels behave very similarly. At about 0630 UT both channels see a distinct increase in the flux. Another nearly identical flux enhancement is seen in the lowest energy channel at about 1130 UT (but not so clearly in the higher energy channel). At about 16 UT the electron fluxes start increasing strongly in both channels reaching maxima around 18 UT. The electron fluxes at NOAA-15 (not shown) remain clearly below those of NOAA-16 but roughly follow the same temporal evolution. In particular, the absolute maximum at NOAA-15 is also seen at about 18 UT. The L shell of maximum electron flux at NOAA-16 (not shown) decreases in the beginning of the day and reaches its minimum already before 06 UT, the lowest energy electron channel interestingly at the same time as the lowest energy ions. On the other hand, the corresponding L shell at the absolute flux maximum before 18 UT took place at a significantly higher L shell of about 5-6.

3.3. CLUSTER Observations

The four Cluster satellites had their perigee at about 07 UT on March 31, 2001. The RAPID energetic particle spectrometer [Wilken et al., 1997; 2001] measured the electron fluxes around the perigee since about 0630 UT (see Figure 8) and the three types of ions (protons, heliums and oxygens) since about 0810 UT. Curiously, the Cluster perigee was in the 22 LT sector, i.e., in between the LT sectors of the two NOAA satellites. Cluster observed the highest flux of energetic electrons around the perigee from 0635 UT to 0740 UT which corresponds L-shells from about 4 to 5. This is in an excellent agreement with NOAA-16 and NOAA-15 (see Figures 4 and 6) observations where the highest fluxes were restricted to below L=5. After a weak minimum at about L=5-6 Cluster observed a region of lower fluxes of energetic electrons until about L=12. This structure can also be seen by NOAA-16 at about 05 UT (not shown), as well as at NOAA-15 already at 04 UT and also later at about 08 UT, i.e., at the time of Cluster observations.

Figure 9 shows the ion composition data from the Cluster/CIS instrument which started operating at about 0640 UT when the Cluster satellites were still flying to lower L-shells. The CIS data shows consistent and overwhelming O⁺ dominance at L=4-6. The upper energy limit of CIS instrument is 40 keV and the particle spectra (not shown) show that the intensity maximum of oxygen ions is at or above this upper limit. From about 08 UT Cluster satellites are in the plasmashet where the ions appear in bursty flows and have a lower average energy than in the ring current. However, CIS data shows that also the bursty plasmashet fluxes are dominated by oxygen ions.

4. DISCUSSION AND CONCLUSIONS

The ring current particle population was found to be greatly intensified from the average quiet time level during the storm. The ion flux maximum was coinciding with the main phase when the Dst index was decreasing most rapidly with time. This maximum was seen as particularly strong enhancements of the ion fluxes in the post midnight and dusk sectors around 06 UT. The behavior of the lowest ion energy channel and the CIS ion composition data in the overlapping energy interval confirm that the ring current was dominated by oxygen ions in the main phase of the storm. The NOAA data also show that the outflow of oxygen ions very probably started already in the beginning of the main phase and reached its maximum at about 0430 UT in the night side and around 06 UT in the dusk sector.

The very intense ion enhancement at the lowest energy channel observed by NOAA-15 at about 0630 UT cannot be only explained by the drift of previously existing population from the night side because the fluxes observed by NOAA-16 are lower than those by NOAA-15. Instead, the

enhancement is well in agreement with the simultaneous observation of intense ionospheric outflow of low energy oxygen ions at the dusk by the FAST satellite [see *Baker et al.*, 2002]. Furthermore the Cluster satellites observed an overwhelming O^+ dominance around 40 keV in the pre-midnight sector. All these additional observations give further evidence for the fact that the majority of ions observed by the NOAA satellites during the storm main phase are oxygen ions which dominate at least in the low-energy part of the ring current.

Note also that the NOAA-16 low-energy ions reached their maximum clearly before the higher energy ions. This further implies a different acceleration mechanism for the low-energy ions (oxygen) that most likely are accelerated during their upwelling from the ionosphere and the high-energy ions that rather depict evidence for an injection. The fluxes observed by NOAA-16 at about 0630 UT probably result from a strong dispersionless (at least at this time resolution) substorm injection. This is confirmed by the similar signatures in NOAA-16 ion and electron data (see Figures 3 and 7). This kind of coherent signature is not seen at dusk by NOAA-15. Thus after the injection at 0630 UT in the night side the ions started drifting westwards and electrons eastwards. These injected ions were seen by NOAA-15 at about 0730 UT in the dusk in the energy range of 80-250 keV. The higher energy ions drifted westwards faster and were missed by NOAA-15 which was only flying towards the relevant low L shells.

We would also like to note that NOAA-15 detected a simultaneous strong low-energy ion enhancement in the morning sector at about 07 UT (not shown). This enhancement can not be understood in terms of drift but rather supports the view that it results from the above mentioned ionospheric outflow of oxygen ions. It has been reported [*Daglis*, 1997] that oxygen can be the main ion species in the RC during the main phase of great magnetic storms. Also, the fraction of oxygen in RC is the larger the more intense the storm is. Our observations further emphasize the view that the ionospheric outflow of oxygen is a global phenomenon, and that the observed enhanced ion fluxes had a large oxygen fraction. Also, our results suggest that there is a large contribution to the low-energy part of the ring current during storm main phase which comes directly from the ionosphere instead of a less direct route via storage and acceleration in the tail and subsequent drift.

The particle flux peaks were found to proceed to successively low L shells down to about $L=2.8$ during the storm main phase. Note that very similar L shells were found for NOAA-16 and NOAA-15 both for ions and electrons. The low L value is also supported by the fact that the AE index was relatively quiet while the Kp index was at its highest during the largest ion fluxes at about 06 UT. Note also that the obtained minimum L value of 2.8 agrees very well with the size of the present storm and the earlier detected rela-

tion between storm size and RC flux maxima [*Hamilton et al.*, 1988].

In a dramatic difference to ions, the energetic electrons had their maximum fluxes only in the recovery phase of the storm. The largest electron fluxes were found by NOAA-16 in the night sector. The NOAA-15 fluxes at dawn (not shown) can be well understood in terms of the standard view of eastward drift of electrons. These and other facts suggest that the flux maxima of low-energy ions and energetic electrons were formed by different mechanisms, the electron flux maxima at 16-18 UT by the standard tailside storage and acceleration, the ion maxima at 06-08 UT mainly by the field-aligned acceleration of ionospheric ions. Note also that the largest values of the AE index at 16-18 UT (see Figure 1) coincide very well with the electron flux maximum. This is also in accordance with the found larger L value of about 5-6 of the maximum fluxes at this time, implying that the injections occurred at L shells higher than the ring current maxima during the main phase. (Note also that this enhancement coincides, taking roughly 1h-delay between ACE and NOAA, with the start of enhanced solar wind pressure and IMF Bz turning slightly less negative after a prolonged period of strongly negative values. These conditions favor substorm occurrence.)

The 06 UT field-aligned acceleration can not be due to a static potential since it would operate similarly with electrons and ions of different masses, and NOAA satellites do not see similar fluxes of energetic electrons at dusk. We suggest that the field-aligned acceleration is caused by the ion cyclotron mechanism which accelerates only ions and prefers heavy ions like oxygens. Equatorially generated ion cyclotron waves (short period Alfvén waves) below the proton gyrofrequency propagate into the ionosphere and cause transverse acceleration of oxygen ions by ion cyclotron instability. This is possible at the fairly low latitudes where the ionospheric gyrofrequency of oxygen ions is close to the equatorial gyrofrequency of protons. Note that this mechanism would mainly accelerate oxygens and less protons, in agreement with our observations. Moreover, it has been found that ion cyclotron wave activity is greatly enhanced during the storm main phase even at ionospheric altitudes [*Bräysy et al.*, 1998], giving support for the existence of these waves and the suggested mechanism.

Acknowledgments. We greatly acknowledge the financial support by the Academy of Finland.

REFERENCES

Baker, D.N., Ergun, R.E., Burch, J.L., Jahn, J-M., Daly, P.W., Friedel, R., Reeves, G.D., Fritz, T.A., and Mitchell, D.G, A telescopic and microscopic view of a magnetospheric substorm on 31 March 2001, *Geophys. Res. Lett.*, doi: 10.1029/2001GL014491, 2002

- Bräysy, T., Mursula, K. and Marklund, G., Ion cyclotron waves during a great magnetic storm observed by Freja double-probe electric field instrument, *J. Geophys. Res.*, *103*, 4145, 1998
- Daglis, I.A., The role of magnetosphere-ionosphere coupling in magnetic storm dynamics, in *Magnetic Storms, Geophysical Monograph*, *98*, 107, edited by B.T. Tsurutani et al., AGU, Washington, D.C., 1997
- Evans, D.S. and Greer, M.S., Polar orbiting environmental satellite space environment monitor - 2: instrument descriptions and archive data documentation, *NOAA Technical Memorandum OAR SEC-93*, Boulder, Colorado, 2000
- Hamilton, D.C., Gloeckler, G., Ipavich, F.M., Stüdemann, W., Wilken, B., and Kremser, G., Ring current development during the great geomagnetic storm of February 1986, *J. Geophys. Res.*, *102*, 14113, 1997
- Korth, A., and Friedel, R.H.W., Dynamics of energetic ions and electrons between L=2.5 and L=7 during magnetic storms, *J. Geophys. Res.*, *102*, 14113, 1997
- Smith, P. H., and Hoffman, R. A., Ring current particle distributions during the magnetic storms of December 16-18, 1971, *J. Geophys. Res.*, *78*, 4731, 1973
- Réme, H., J.M. Bosqued, J.A. Sauvaud et al., The Cluster Ion Spectrometry (CIS) Experiment, *Space Science Reviews*, *79*, 303-350, 1997
- Søråas, F., K. Aarsnes, K. Oksavik and D.S. Evans, Ring current intensity estimated from low-altitude proton observations, *J. Geophys. Res.*, *107*, 101029, 2002
- Wilken, B., et al., RAPID: The Imaging Energetic Particle Spectrometer on Cluster, *Space Sci. Rev.*, *79*, 399, 1997
- Wilken, B., et al., First results from the RAPID imaging energetic particle spectrometer on board Cluster, *Annales Geophysicae*, *19*, 1355, 2001.

FIGURE CAPTIONS

Figure 1. From top to bottom: ACE observations of the IMF Bz(GSM) component, solar wind velocity, solar wind pressure together with Dst and AE indices on March 31, 2001.

Figure 2. NOAA-16 total ion and electron fluxes on 30-31 March, 2001.

Figure 3. NOAA-16 maximum ion fluxes in the three lowest energy channels. One point denotes the maximum during one night side passes.

Figure 4. The L values of the maximum flux of NOAA-16 ions in the three lowest energy channels for each nightside pass.

Figure 5. The same for NOAA-15 as Figure 3 for NOAA-16.

Figure 6. The same for NOAA-15 as Figure 4 for NOAA-16.

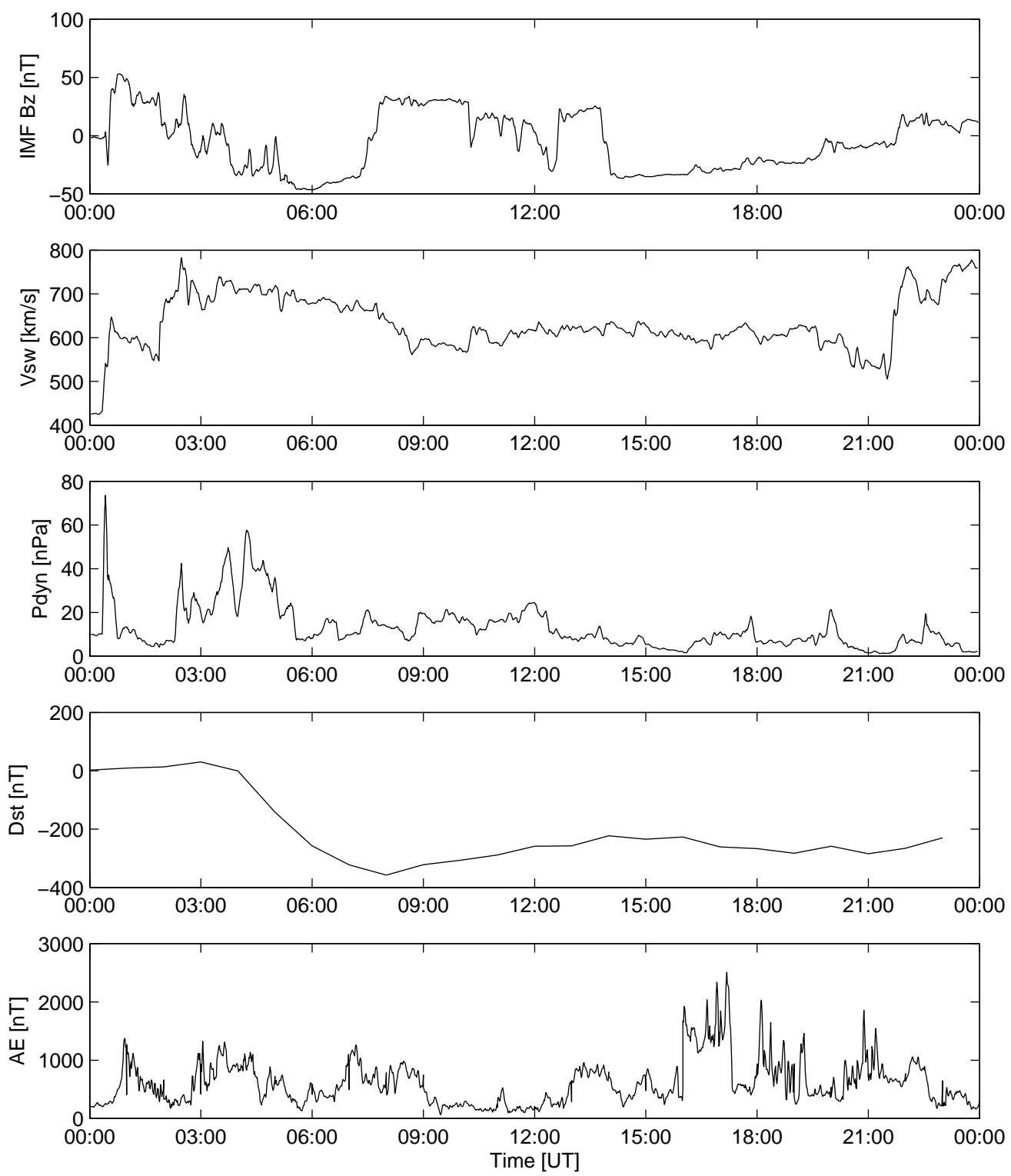
Figure 7. NOAA-16 maximum electron fluxes in the two lowest energy channels. One point denotes the maximum during one night side passes.

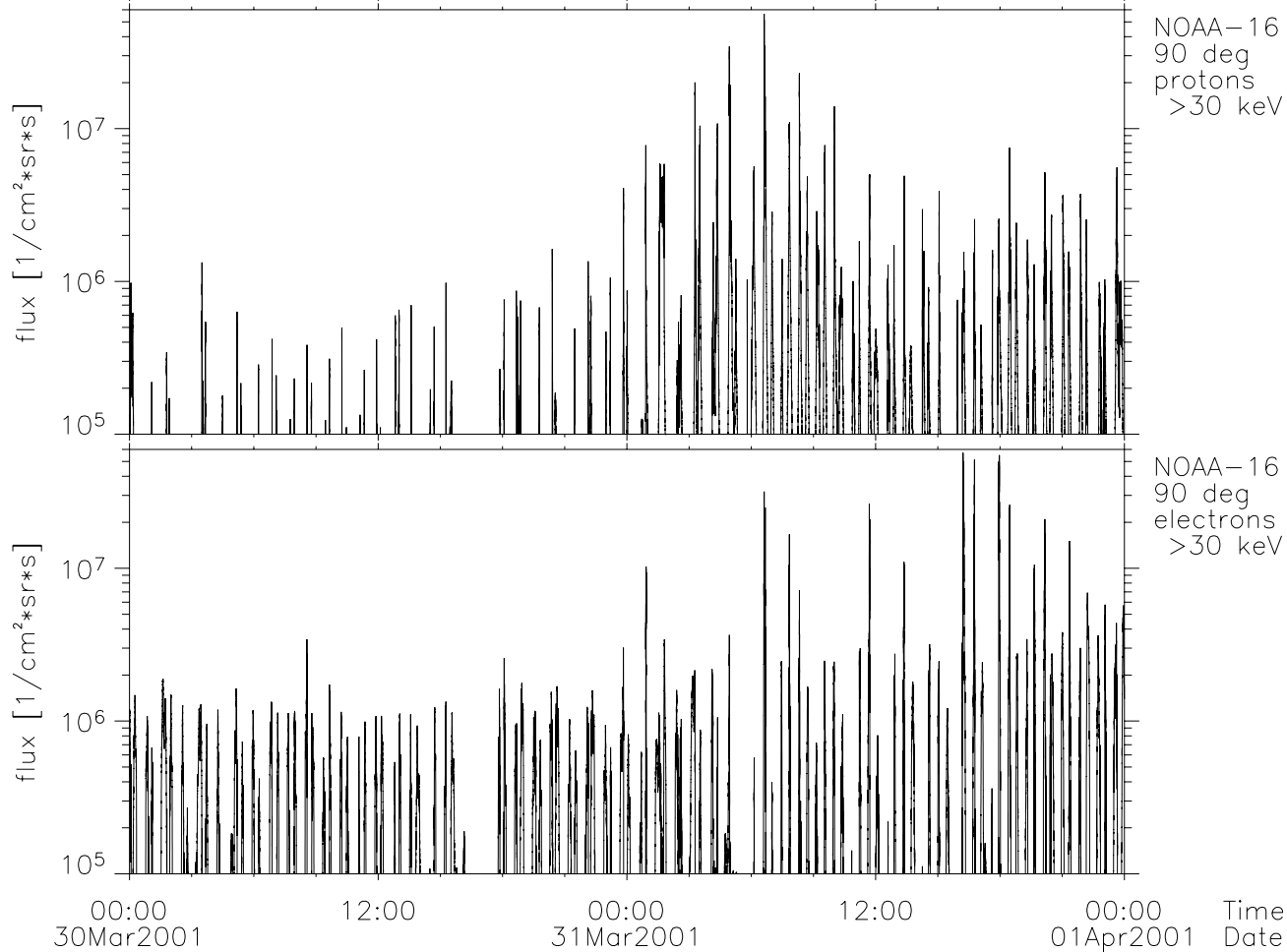
Figure 8. Cluster s/c1 RAPID total fluxes of energetic electrons, protons and oxygens ($\text{s}^{-1}\text{cm}^{-2}\text{sr}^{-1}\text{keV}^{-1}$).

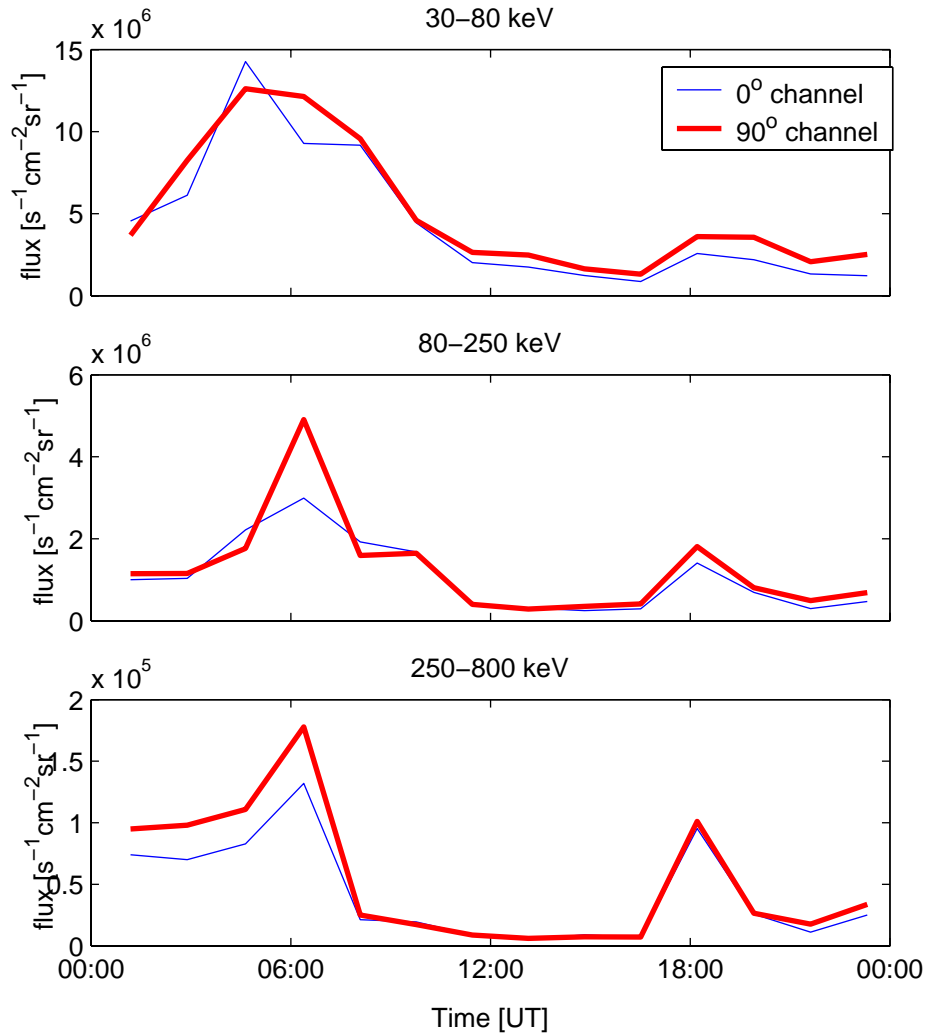
Figure 9. Total number density of Cluster s/c1 CIS protons, helium and oxygen ions.

GLOBAL VIEW OF ENERGETIC PARTICLES

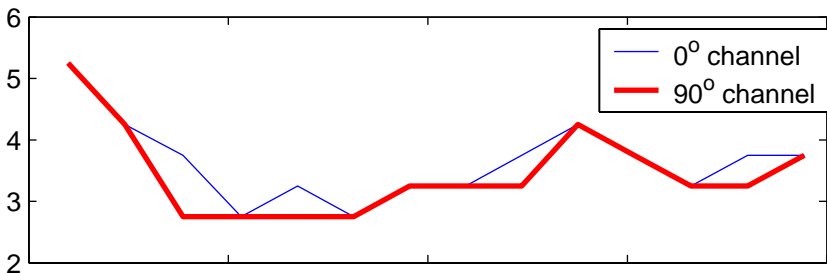
ASIKAINEN, T, KERTTULA, R., MURSULA, K.



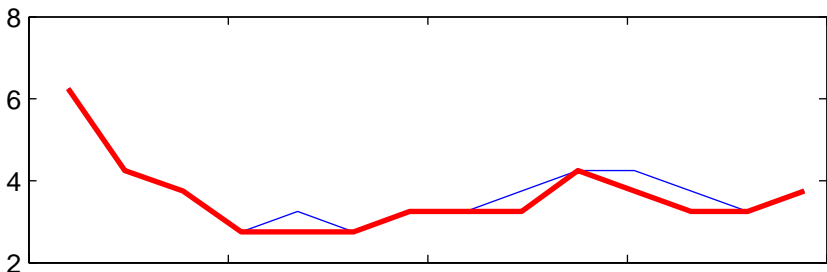




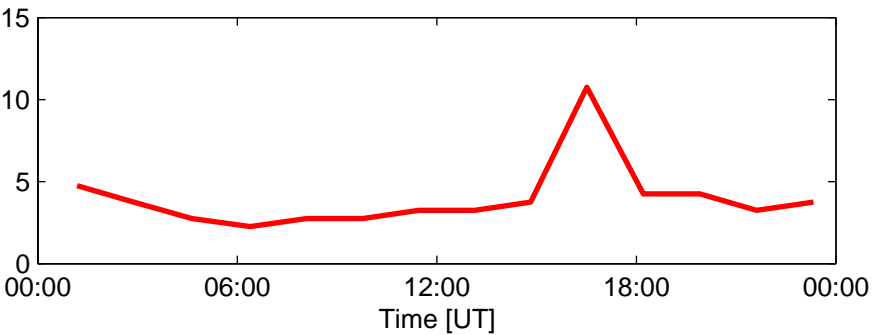
30–80 keV

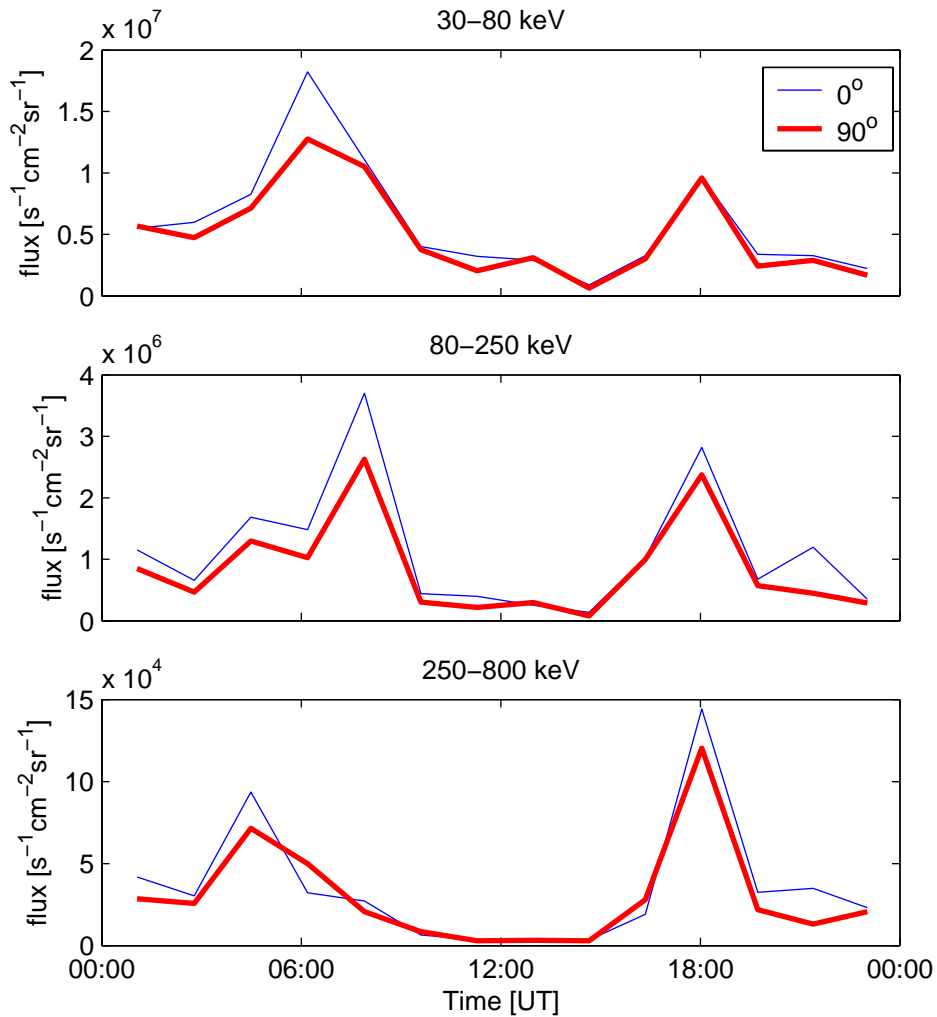


80–250 keV

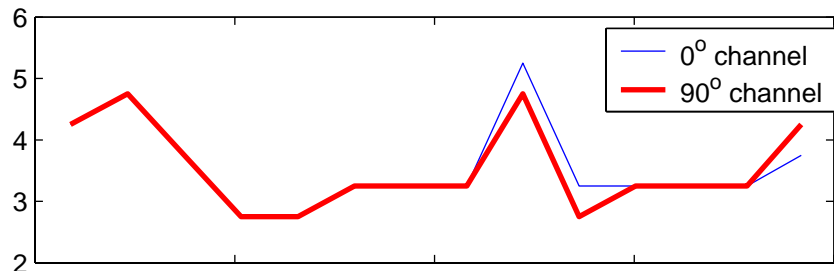


250–800 keV

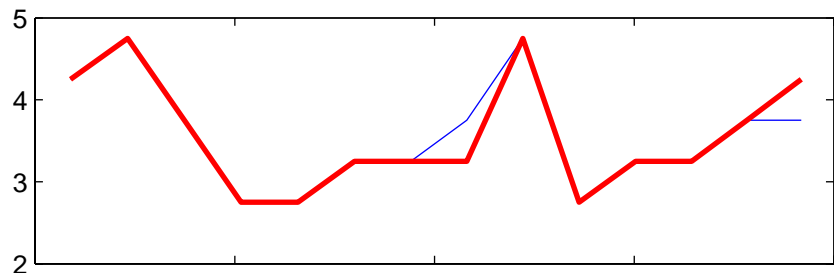




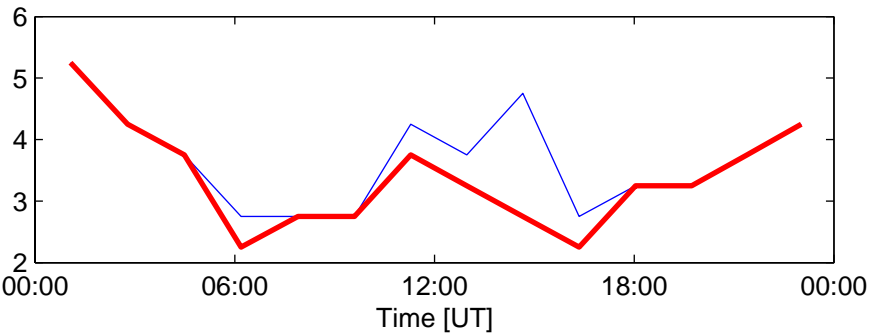
30–80 keV

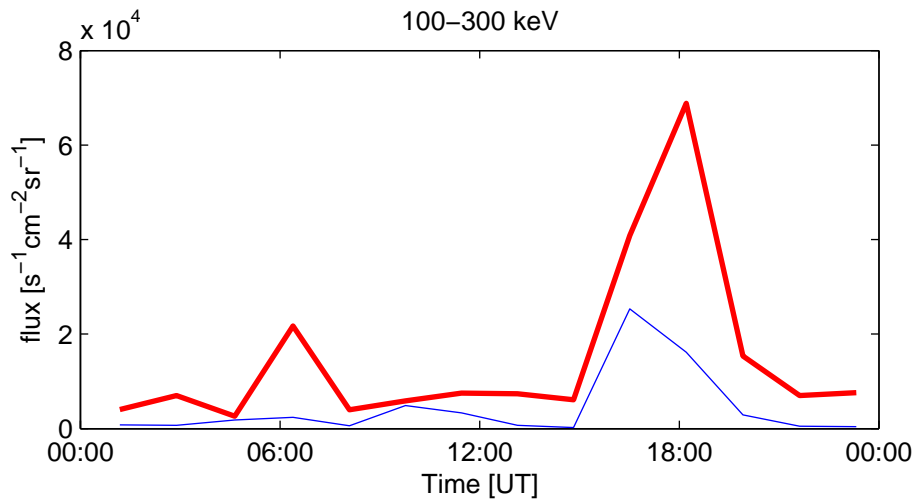
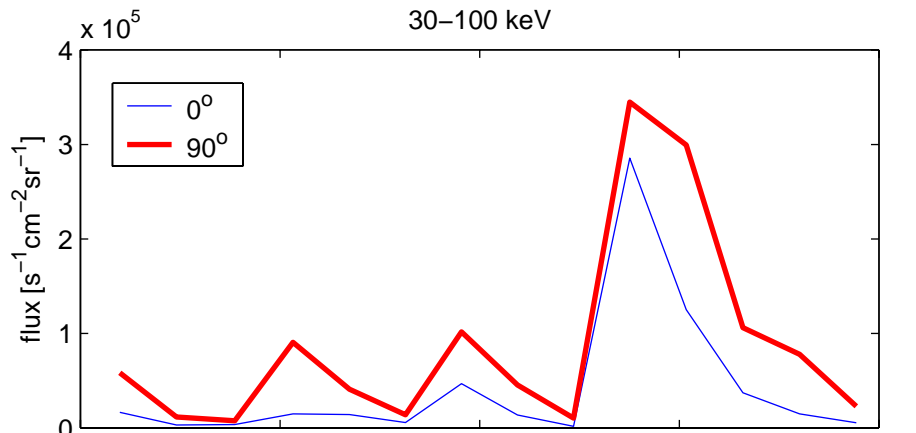


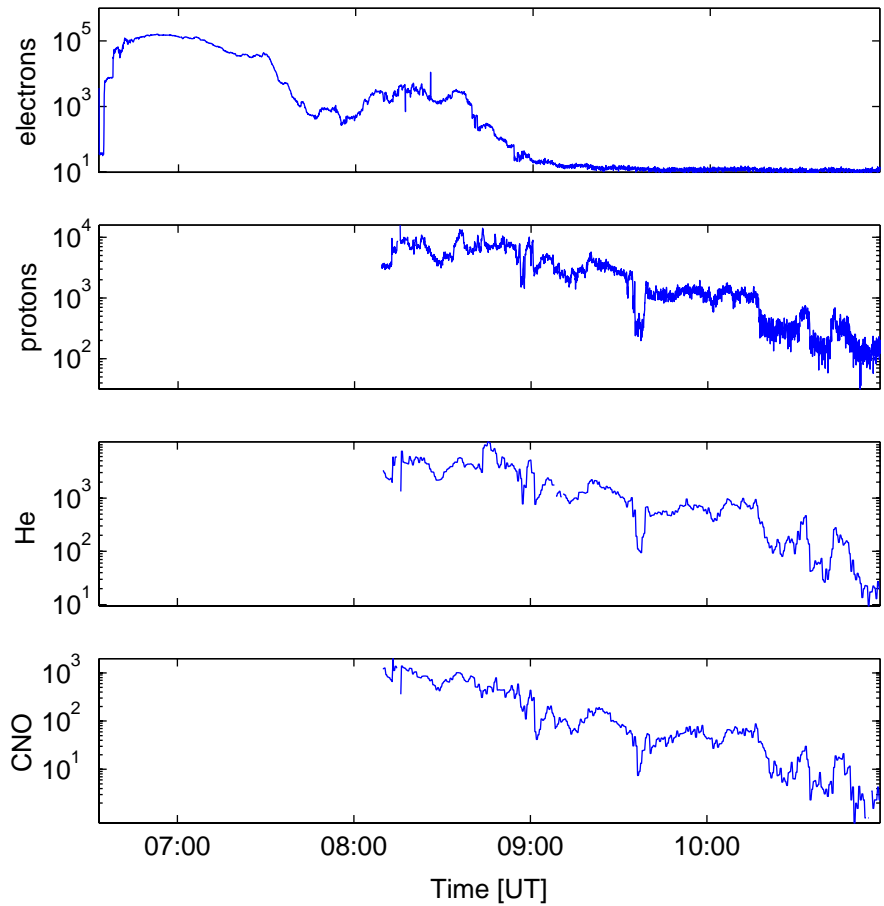
80–250 keV



250–800 keV







CIS/CODIF ion data

